Journal of Control, Automation and Electrical Systems
https://doi.org/10.1007/s40313-021-00778-x

Modeling and Nonlinear Control Utilizing Unit Complex Numbers

Fabio Bobrow[1] · **Bruno Augusto Angélico**[1] · **Paulo Sérgio Pereira da Silva**[1]

Received: 3 March 2021 / Revised: 24 May 2021 / Accepted: 12 July 2021

Abstract
This paper covers the modeling and nonlinear control of the mechanical systems where instead of angle coordinates, unit complex numbers are used as control states. This approach is useful not only to get rid of trigonometric functions, but mainly because it is a specific case of the 3D configuration that utilizes unit hypercomplex numbers (quaternions) as system states, and therefore facilitates its understanding, which represents a contribution to control education. As an example of application, it is considered a particular case of a cube balanced on one of its edges, which is equivalent to a reaction wheel inverted pendulum. The derived nonlinear control law is equivalent to a linear one and is characterized by only three straightforward tuning parameters. Experimental results are presented to validate modeling and control.

Keywords Complex numbers · Nonlinear control · Reaction wheel inverted pendulum

1 Introduction

Unit complex numbers (Fig. 1), represented here as $q = (q_0 + i\, q_1)$, also called unit circle $\mathbb{S}^1$, circle group $\mathbb{T}^1$ or special orthogonal group $SO(2)$, are the multiplicative group of all complex numbers with absolute value 1. They form a commutative compact Lie Group, with planar 2D rotation employed as a group operator, which is well known and has been employed in several fields, for instance, to describe the synchronization behavior of Kuramoto oscillators (Chopra and Spong 2005; Bosso et al. 2019).

Inverted pendulum systems have been a popular demonstration of using feedback control to stabilize open-loop unstable systems. Introduced back in 1908 by Stephenson (1908), the first solution to this problem was presented only in 1960 with Roberge (1960) and it is still widely used to test, demonstrate and benchmark new control concepts and theories (Xu et al. 2013; Yang et al. 2014; Shi et al. 2015; Wang et al. 2017; Guaracy et al. 2017).

Differently from cart-pole inverted pendulums, which have a controlled cart with linear motion (Fig. 2a), reaction wheel pendulums have a controlled rotating wheel that exchanges angular momentum with the pendulum (Fig. 2b). First introduced in 2001 by Spong et al. (2001), it was soon adapted to 3D design variants (Sanyal et al. 2004; Lee and Goswami 2007).

Perhaps, the most notable of them is the Cubli. Originally developed and baptized in 2012 by Gajamohan et al. (2012, 2013) and Muehlebach et al. (2013); Muehlebach and DAndrea (2017) from the Institute for Dynamic Systems and Control of Zurich Federal Institute of Technology (ETH Zurich), the Cubli is a device that consists of a cube with three reaction wheels mounted on orthogonal faces. By positioning the Cubli on its edge, it becomes a reaction wheel-based 1D inverted pendulum (Fig. 3a), while if it is positioned on its vertex, it becomes a reaction wheel-based 3D inverted pendulum (Fig. 3b).

The purpose of this paper is to model the 1D configuration of the Cubli, resulting in a system equivalent to the scheme presented in Fig. 2b, and then design and implement a nonlinear controller for it. Although this is widely available in the literature, with different control techniques such as feedback linearization with partial feedback linearization (Fantoni et al. 2001), energy and passivity-based approach

Supplementary Information The online version contains supplementary material available at https://doi.org/10.1007/s40313-021-00778-x.

✉ Fabio Bobrow
fbob@usp.br

Bruno Augusto Angélico
angelico@lac.usp.br

Paulo Sérgio Pereira da Silva
paulo@lac.usp.br

[1] Department of Telecommunication and Control Engineering, Escola Politécnica, University of São Paulo USP, São Paulo, SP, Brazil

Published online: 13 August 2021

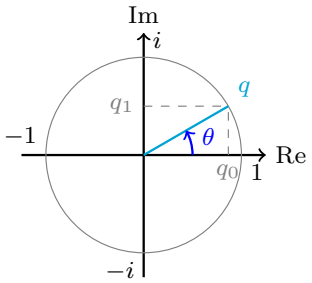

Fig. 1 Unit complex number

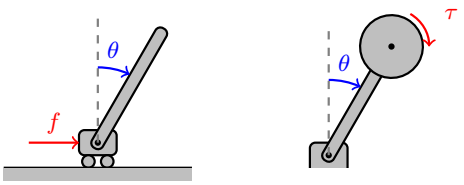

(a) Cart-pole **(b)** Reaction wheel

Fig. 2 Inverted pendulum types

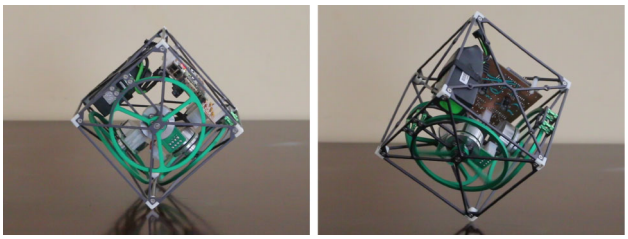

(a) Edge - 1D **(b)** Vertex - 3D

Fig. 3 Cubli

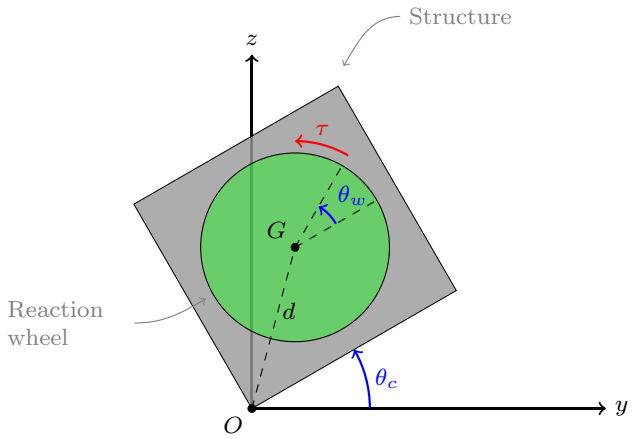

Fig. 4 Cubli schematic diagram

Table 1 The Cubli parameters

Parameter	Value
l	0.15 m
m_s	0.70 kg
m_w	0.15 kg
I_{sG}	3.75×10^{-3} kg·m^2
I_{wG}	1.25×10^{-4} kg·m^2

(Spong et al. 2001), observer-based feedback stabilizing controller (Jepsen et al. 2009), variable structure control with forced sliding mode (Andrievsky 2011) and linear matrix inequalities (Gritli and Belghith 2018), to cite a few, the approach in this paper utilizes unit complex numbers as control states instead of angles, which represents a didactic contribution to control education.

Besides, the approach considered here facilitates the understanding of hypercomplex numbers (quaternions) as system states in modeling and control. In the 3D case with quaternions representation, the unit circle $\mathbb{S}^1$ in $\mathbb{R}^2$ is replaced by the unit 3-sphere $\mathbb{S}^3$ in $\mathbb{R}^4$, which cannot be easily visualized in our 3D world. Moreover, they are a non-commutative compact Lie Group.

2 System Modeling

This section firstly defines the system model considering angular variables and further transform it to the notation of unit complex numbers.

The Cubli balancing on its edge is composed of two rigid bodies: a structure and a reaction wheel (Fig. 4). The structure rotates freely around the pivot point O (articulation edge), while the reaction wheel, besides rotating together with the structure, also rotates around its center of mass G (axial axis).

The variables θ_c and ω_c denote the structure angular displacement and velocity, while θ_w and ω_w denote the reaction wheel relative (measured with respect to the structure) angular displacement and velocity, respectively.

Regarding the structure, l denotes the side length, m_s denotes the mass, and I_{sG} denotes the structure moment of inertia around its center of mass G. For the reaction wheel, m_w denotes the mass and I_{wG} the moment of inertia around its center of mass G. These parameters were obtained from the CAD version of the Cubli and are given in Table 1.

The constant $d = \frac{l\sqrt{2}}{2}$ is the distance between the pivot point O and structure/reaction wheel center of mass G, $I_{sO} = I_{sG} + m_s d^2$ and $I_{wO} = I_{wG} + m_w d^2$ are the structure and reaction wheel moment of inertia around pivot point O, respectively, whereas $I_{cO} = I_{sO} + I_{wO}$ represents the Cubli total moment of inertia around pivot point O. The Cubli total mass is given $m_c = m_s + m_w$ and g denotes the acceleration of gravity.

2.1 Kinetic Energy

The structure kinetic energy T_s is given by:

$$\begin{aligned} T_s &= \frac{1}{2} I_{\mathrm{s_G}} \dot{\theta}_{\mathrm{c}}^2 + \frac{1}{2} m_{\mathrm{s}} \left(\mathrm{d}\dot{\theta}_{\mathrm{c}}\right)^2 \\ &= \frac{1}{2} \left(I_{\mathrm{s_G}} \dot{\theta}_{\mathrm{c}}^2 + m_{\mathrm{s}} d^2 \right) \dot{\theta}_{\mathrm{c}}^2 \\ &= \frac{1}{2} I_{\mathrm{s_O}} \dot{\theta}_{\mathrm{c}}^2. \end{aligned} \tag{1}$$

On the other hand, the reaction wheel kinetic energy T_w is given by:

$$\begin{aligned} T_w &= \frac{1}{2} I_{\mathrm{w_G}} \left(\dot{\theta}_{\mathrm{c}}^2 + \dot{\theta}_{\mathrm{w}}^2 \right)^2 + \frac{1}{2} m_{\mathrm{w}} \left(\mathrm{d}\dot{\theta}_{\mathrm{c}}\right)^2 \\ &= \frac{1}{2} I_{\mathrm{w_G}} \left(\dot{\theta}_{\mathrm{c}}^2 + \dot{\theta}_{\mathrm{w}}^2 \right)^2 + \frac{1}{2} m_{\mathrm{w}} d^2 \dot{\theta}_{\mathrm{c}}^2 \\ &= \frac{1}{2} I_{\mathrm{w_G}} \left(\dot{\theta}_{\mathrm{c}}^2 + \dot{\theta}_{\mathrm{w}}^2 \right)^2 + \frac{1}{2} \left(I_{\mathrm{w_O}} - I_{\mathrm{w_G}} \right) \dot{\theta}_{\mathrm{c}}^2. \end{aligned} \tag{2}$$

Thus, the Cubli total kinetic energy T is the sum of Eqs. (1) and (2), such that:

$$\begin{aligned} T &= \frac{1}{2} I_{\mathrm{s_O}} \dot{\theta}_{\mathrm{c}}^2 + \frac{1}{2} I_{\mathrm{w_G}} \left(\dot{\theta}_{\mathrm{c}}^2 + \dot{\theta}_{\mathrm{w}}^2 \right)^2 + \frac{1}{2} \left(I_{\mathrm{w_O}} - I_{\mathrm{w_G}} \right) \dot{\theta}_{\mathrm{c}}^2 \\ &= \frac{1}{2} \left(I_{\mathrm{s_O}} + I_{\mathrm{w_O}} - I_{\mathrm{w_G}} \right) \dot{\theta}_{\mathrm{c}}^2 + \frac{1}{2} I_{\mathrm{w_G}} \left(\dot{\theta}_{\mathrm{c}}^2 + \dot{\theta}_{\mathrm{w}}^2 \right)^2 \\ &= \frac{1}{2} \left(I_{c_O} - I_{\mathrm{w_G}} \right) \dot{\theta}_{\mathrm{c}}^2 + \frac{1}{2} I_{\mathrm{w_G}} \left(\dot{\theta}_{\mathrm{c}}^2 + \dot{\theta}_{\mathrm{w}}^2 \right)^2 \\ &= \frac{1}{2} \bar{I}_{\mathrm{c_O}} \dot{\theta}_{\mathrm{c}}^2 + \frac{1}{2} I_{\mathrm{w_G}} \left(\dot{\theta}_{\mathrm{c}}^2 + \dot{\theta}_{\mathrm{w}}^2 \right)^2, \end{aligned} \tag{3}$$

where $\bar{I}_{\mathrm{c_O}} = I_{c_O} - I_{\mathrm{w_G}}$ is the Cubli total moment of inertia around pivot point O without considering the contribution of the reaction wheel.

2.2 Potential Energy

The structure potential energy V_s is given by:

$$V_s = m_{\mathrm{s}} g\, d \sin\left(\theta_{\mathrm{c}} + \frac{\pi}{4}\right), \tag{4}$$

whereas the reaction wheel potential energy V_w is given by:

$$V_w = m_{\mathrm{w}} g\, d \sin\left(\theta_{\mathrm{c}} + \frac{\pi}{4}\right). \tag{5}$$

Thus, the Cubli total potential energy V is the sum of Eqs. (4) and (5):

$$\begin{aligned} V_s &= m_{\mathrm{s}} g\, d \sin\left(\theta_{\mathrm{c}} + \frac{\pi}{4}\right) + m_{\mathrm{w}} g\, d \sin\left(\theta_{\mathrm{c}} + \frac{\pi}{4}\right) \\ &= \left(m_{\mathrm{s}} + m_{\mathrm{w}}\right) g\, d \sin\left(\theta_{\mathrm{c}} + \frac{\pi}{4}\right) \\ &= m_{\mathrm{c}} g\, d \sin\left(\theta_{\mathrm{c}} + \frac{\pi}{4}\right). \end{aligned} \tag{6}$$

2.3 Equations of Motion

Once the kinetic and potential energies have been defined, the equations of motion can be derived utilizing the Lagrange method. Let τ denote the input torque of the motor and $\tau_{\mathrm{f}}(\dot{\theta}_{\mathrm{w}})$ the nonlinear friction torque of the motor (to be detailed further). For the generalized coordinate θ_{c}:

$$\begin{aligned} &\frac{\mathrm{d}}{\mathrm{d}t} \left(\frac{\partial T}{\partial \dot{\theta}_{\mathrm{c}}} \right) - \frac{\partial T}{\partial \theta_{\mathrm{c}}} + \frac{\partial V}{\partial \theta_{\mathrm{c}}} = Q_{\theta_{\mathrm{c}}}, \\ &\bar{I}_{\mathrm{c_O}} \ddot{\theta}_c^2 + I_{\mathrm{w_G}} \left(\ddot{\theta}_c^2 + \ddot{\theta}_w^2 \right) + m_{\mathrm{c}} g\, d \cos\theta_{\mathrm{c}} = 0. \end{aligned} \tag{7}$$

For the generalized coordinate θ_{w}:

$$\begin{aligned} &\frac{\mathrm{d}}{\mathrm{d}t} \left(\frac{\partial T}{\partial \dot{\theta}_{\mathrm{w}}} \right) - \frac{\partial T}{\partial \theta_{\mathrm{w}}} + \frac{\partial V}{\partial \theta_{\mathrm{w}}} = Q_{\theta_{\mathrm{w}}}, \\ &I_{\mathrm{w_G}} \left(\ddot{\theta}_c^2 + \ddot{\theta}_w^2 \right) = -\tau_{\mathrm{f}}(\dot{\theta}_{\mathrm{w}}) + \tau. \end{aligned} \tag{8}$$

Equations (7) and (8) represent the equation of motion for the equivalent reaction wheel inverted pendulum. They can be written together in matrix notation, such that:

$$\begin{bmatrix} \bar{I}_{\mathrm{c_O}} & I_{\mathrm{w_G}} \\ 0 & I_{\mathrm{w_G}} \end{bmatrix} \begin{bmatrix} \ddot{\theta}_c^2 \\ \ddot{\theta}_c^2 + \ddot{\theta}_w^2 \end{bmatrix} = \begin{bmatrix} -m_{\mathrm{c}} g\, d \cos\theta_{\mathrm{c}} \\ -\tau_{\mathrm{f}}(\dot{\theta}_{\mathrm{w}}) + \tau \end{bmatrix}. \tag{9}$$

Isolating the time derivative terms:

$$\begin{aligned} \begin{bmatrix} \ddot{\theta}_c^2 \\ \ddot{\theta}_c^2 + \ddot{\theta}_w^2 \end{bmatrix} &= \begin{bmatrix} \bar{I}_{\mathrm{c_O}} & I_{\mathrm{w_G}} \\ 0 & I_{\mathrm{w_G}} \end{bmatrix}^{-1} \begin{bmatrix} -m_{\mathrm{c}} g\, d \cos\theta_{\mathrm{c}} \\ -\tau_{\mathrm{f}}(\dot{\theta}_{\mathrm{w}}) + \tau \end{bmatrix} \\ &= \begin{bmatrix} \frac{1}{\bar{I}_{\mathrm{c_O}}} & -\frac{1}{\bar{I}_{\mathrm{c_O}}} \\ 0 & \frac{1}{I_{\mathrm{w_G}}} \end{bmatrix} \begin{bmatrix} -m_{\mathrm{c}} g\, d \cos\theta_{\mathrm{c}} \\ -\tau_{\mathrm{f}}(\dot{\theta}_{\mathrm{w}}) + \tau \end{bmatrix} \\ &= \begin{bmatrix} \frac{1}{\bar{I}_{\mathrm{c_O}}} \left(-m_{\mathrm{c}} g\, d \cos\theta_{\mathrm{c}} + \tau_{\mathrm{f}}(\dot{\theta}_{\mathrm{w}}) - \tau \right) \\ \frac{1}{I_{\mathrm{w_G}}} \left(-\tau_{\mathrm{f}}(\dot{\theta}_{\mathrm{w}}) + \tau \right) \end{bmatrix}. \end{aligned} \tag{10}$$

Because the total moment of inertia is significantly larger than the reaction wheel moment of inertia ($\bar{I}_{\mathrm{c_O}} \gg I_{\mathrm{w_G}}$), the reaction wheel angular acceleration will be significantly larger than the structure angular acceleration ($\ddot{\theta}_w \gg \ddot{\theta}_c$).

The final system model is given by:

$$\begin{cases} \dot{\theta}_{\mathrm{c}} = \omega_{\mathrm{c}} \\ \dot{\theta}_{\mathrm{w}} = \omega_{\mathrm{w}} \\ \dot{\omega}_{\mathrm{c}} = \frac{1}{\bar{I}_{\mathrm{c_O}}} \left(-m_{\mathrm{c}} g\, d \cos\theta_{\mathrm{c}} + \tau_{\mathrm{f}}(\omega_{\mathrm{w}}) - \tau \right) \\ \dot{\omega}_{\mathrm{w}} = \frac{1}{I_{\mathrm{w_G}}} \left(-\tau_{\mathrm{f}}(\omega_{\mathrm{w}}) + \tau \right) \end{cases}. \tag{11}$$

This set of equations can be represented as the block diagram of Fig. 5, from where it is easier to interpret the gravity torque and motor friction terms.

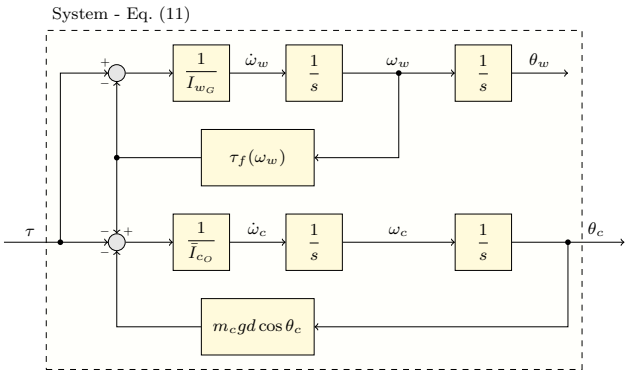

Fig. 5 Cubli dynamics

It is interesting to note that the input torque and motor friction are the terms coupling the Cubli and the reaction wheel dynamics.

3 Unit Complex Numbers

Instead of using the angle θ_c to describe the Cubli orientation, a unit complex number q will be considered.

3.1 Complex Number Notation

A complex number q is a set of two parameters, a real part q_0 and an imaginary part q_1, such that $q = q_0 + q_1 i$, where i stands for the imaginary unit, satisfying $i^2 = -1$. In vector notation, $q = \begin{bmatrix} q_0 & q_1 \end{bmatrix}^{\mathrm{T}}$, where its conjugate is defined as $\bar{q} = \begin{bmatrix} q_0 & -q_1 \end{bmatrix}^{\mathrm{T}}$, and its norm as:

$$|q| = \sqrt{q^{\mathrm{T}} q} = \sqrt{q_0^2 + q_1^2}. \tag{12}$$

3.2 Complex Number Product

It is easy to see that the product of two complex numbers q and r (represented by the $\circ$ operator) is given by:

$$q \circ r = \begin{bmatrix} q_0 r_0 - q_1 r_1 \\ q_0 r_1 + q_1 r_0 \end{bmatrix} = \underbrace{\begin{bmatrix} q_0 & -q_1 \\ q_1 & q_0 \end{bmatrix}}_{R(q)} \begin{bmatrix} r_0 \\ r_1 \end{bmatrix}, \tag{13}$$

where

$$R(q) = \begin{bmatrix} | & | \\ q & G(q)^{\mathrm{T}} \\ | & | \end{bmatrix}, \tag{14}$$

and

$$G(q) = \begin{bmatrix} -q_1 & q_0 \end{bmatrix}. \tag{15}$$

From Eq. (13), it turns out that:

$$q \circ \bar{q} = \bar{q} \circ q = \begin{bmatrix} |q|^2 \\ 0 \end{bmatrix}, \tag{16}$$

and if the complex number has unitary norm ($|q| = 1$), i.e., it is a unit complex number, then:

$$q \circ \bar{q} = \bar{q} \circ q = \begin{bmatrix} 1 \\ 0 \end{bmatrix}. \tag{17}$$

3.3 Unit Complex Number

Let q be a unit complex number. Its real and imaginary parts depend only on the angle θ with respect to the real axis (Fig. 1):

$$q = \begin{bmatrix} \cos\theta \\ \sin\theta \end{bmatrix}. \tag{18}$$

It means that a unit complex number q is a redundant way of describing a rotational angle θ. Time differentiating Eq. (18) yields:

$$\dot{q} = \begin{bmatrix} -\dot{\theta}\sin\theta \\ \dot{\theta}\cos\theta \end{bmatrix} = \underbrace{\begin{bmatrix} -q_1 \\ q_0 \end{bmatrix}}_{G(q)^{\mathrm{T}}} \omega. \tag{19}$$

This is the rotation kinematic equation utilizing unit complex numbers.

Left multiplying Eq. (19) by $G(q)$, it turns out that:

$$\begin{aligned} \begin{bmatrix} -q_1 & q_0 \end{bmatrix} \begin{bmatrix} \dot{q}_0 \\ \dot{q}_1 \end{bmatrix} &= \begin{bmatrix} -q_1 & q_0 \end{bmatrix} \begin{bmatrix} -q_1 \\ q_0 \end{bmatrix} \omega \\ &= \omega. \end{aligned} \tag{20}$$

Note that:

$$\begin{aligned} \frac{\mathrm{d}}{\mathrm{d}t}\left(q^{\mathrm{T}} q\right) &= \frac{\mathrm{d}}{\mathrm{d}t}(1) \\ \dot{q}^{\mathrm{T}} q + q^{\mathrm{T}} \dot{q} &= 0 \\ 2 q^{\mathrm{T}} \dot{q} &= 0 \\ \begin{bmatrix} q_0 & q_1 \end{bmatrix} \begin{bmatrix} \dot{q}_0 \\ \dot{q}_1 \end{bmatrix} &= 0. \end{aligned} \tag{21}$$

From (20) and (21), one can see that:

$$\begin{bmatrix} q_0 & q_1 \\ -q_1 & q_0 \end{bmatrix} \begin{bmatrix} \dot{q}_0 \\ \dot{q}_1 \end{bmatrix} = \begin{bmatrix} 0 \\ \omega \end{bmatrix}. \tag{22}$$

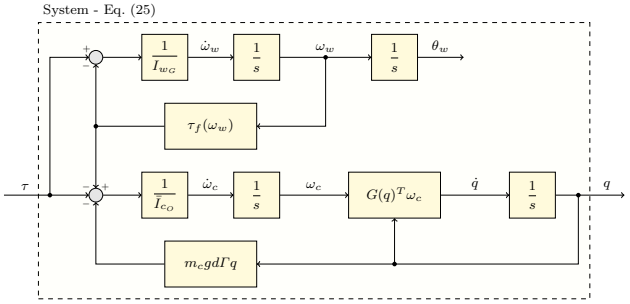

Fig. 6 Cubli dynamics (with unit complex numbers)

Comparing Eq. (22) with (13) results in:

$$\begin{bmatrix} 0 \\ \omega \end{bmatrix} = \bar{q} \circ \dot{q} = \dot{q} \circ \bar{q}, \tag{23}$$

and also in:

$$\begin{bmatrix} 0 \\ \omega \end{bmatrix} = -\dot{\bar{q}} \circ q = -q \circ \dot{\bar{q}}. \tag{24}$$

3.4 Equations of Motion

The Cubli equations of motion from Eq. (11) can be rewritten in terms of unit complex number q as:

$$\begin{cases} \dot{q} = G(q)^{\mathrm{T}} \omega_{\mathrm{c}} \\ \dot{\theta}_{\mathrm{w}} = \omega_{\mathrm{w}} \\ \dot{\omega}_{\mathrm{c}} = \frac{1}{\bar{I}_{\mathrm{cO}}} \left(-m_{\mathrm{c}} g \, d \Gamma q + \tau_{\mathrm{f}}(\omega_{\mathrm{w}}) - \tau \right) \\ \dot{\omega}_{\mathrm{w}} = \frac{1}{I_{\mathrm{wG}}} \left(-\tau_{\mathrm{f}}(\omega_{\mathrm{w}}) + \tau \right) \end{cases}, \tag{25}$$

where $\Gamma = \begin{bmatrix} 1 & 0 \end{bmatrix}$. Despite having one more equation now (since q is a two-dimensional vector), there is no longer any trigonometric function. This set of equations is represented in the block diagram of Fig. 6.

3.5 Linearized Dynamics

When the Cubli is at rest $\omega_{\mathrm{c}} = \theta_{\mathrm{w}} = \omega_{\mathrm{w}} = 0$, perfectly balanced in its unstable equilibrium position $q = q_{\mathrm{u}} = \begin{bmatrix} \frac{\sqrt{2}}{2} & \frac{\sqrt{2}}{2} \end{bmatrix}^{\mathrm{T}}$, the linearized dynamics are:

$$\begin{bmatrix} \dot{q} \\ \dot{\theta}_{\mathrm{w}} \\ \dot{\omega}_{\mathrm{c}} \\ \dot{\omega}_{\mathrm{w}} \end{bmatrix} = \left[\begin{array}{c|c|c|c} 0_{2\times 2} & 0_{2\times 1} & G^{\mathrm{T}}(q_{\mathrm{u}}) & 0_{2\times 1} \\ \hline 0_{1\times 2} & 0 & 0 & 1 \\ \hline -\frac{m_{\mathrm{c}} g d}{\bar{I}_{\mathrm{cO}}} \Gamma & 0 & 0 & \frac{b_{\mathrm{w}}}{\bar{I}_{\mathrm{cO}}} \\ \hline 0_{1\times 2} & 0 & 0 & -\frac{b_{\mathrm{w}}}{I_{\mathrm{wG}}} \end{array}\right] \begin{bmatrix} q \\ \theta_{\mathrm{w}} \\ \omega_{\mathrm{c}} \\ \omega_{\mathrm{w}} \end{bmatrix} + \begin{bmatrix} 0_{2\times 1} \\ 0 \\ -\frac{1}{\bar{I}_{\mathrm{cO}}} \\ \frac{1}{I_{\mathrm{wG}}} \end{bmatrix} \tau. \tag{26}$$

Its characteristic equation is given by:

$$\underbrace{s}_{\substack{\text{u.c.n.} \\ \text{redu.}}} \underbrace{s\,(s+\omega_1)}_{\substack{\text{r.wheel} \\ \text{dynamics}}} \underbrace{\left(s^2 - \omega_0^2\right)}_{\substack{\text{cubli} \\ \text{dynamics}}} = 0, \tag{27}$$

where ω_0 is the natural frequency of the 1D Cubli dynamics and ω_1 is the natural frequency of the reaction wheel dynamics, given by:

$$\omega_0 = \sqrt{\frac{m_{\mathrm{c}} g \, d \frac{\sqrt{2}}{2}}{\bar{I}_{\mathrm{cO}}}}, \qquad \omega_1 = \frac{b_{\mathrm{w}}}{I_{\mathrm{wG}}}. \tag{28}$$

The 1D Cubli in it upper equilibrium is an unstable system due to its poles being located at $\pm\omega_0$, while the reaction wheel is marginally stable due to its poles being located at 0 and $-\omega_1$. Moreover, there is also an extra pole at 0, which is inherited from the kinematic equation, since a unit complex number (u.c.n.) is a redundant way to describe an angle.

The controllability matrix has $\mathrm{rank}(\mathcal{C}) = 4$, while the system has dimension $n = 5$. However, even with $\mathrm{rank}(\mathcal{C}) \neq n$, the system is full controllable since one of the system states is redundant due to its unit complex number representation. In other words, although unit complex numbers are being utilized (which includes an extra redundant state), the system still has 2 d.o.f. and thus, its "physical" dimension remains $n = 4$.

4 Attitude Controller

The control goals are to keep the 1D Cubli in its upper position, compensate for disturbances and keep the wheel speed at zero. Initially, one will focus only on the 1D Cubli dynamics, without concern about controlling the reaction wheel.

4.1 Friction Torque Compensation

The friction torque $\tau_{\mathrm{f}}(\omega_{\mathrm{w}})$ occurs in the opposite direction of the reaction wheel angular velocity ω_{w}, and it corresponds to the Coulomb (static) and viscous (dynamic) friction of the motor. However, because the reaction wheel is hollow, there is also a significant aerodynamic drag. Given that, the friction torque can be approximated to:

$$\tau_{\mathrm{f}}(\omega_{\mathrm{w}}) = \mathrm{sign}(\omega_{\mathrm{w}}) \left[\tau_{\mathrm{c}} + b_{\mathrm{w}} |\omega_{\mathrm{w}}| + c_{\mathrm{d}} |\omega_{\mathrm{w}}|^2 \right], \tag{29}$$

where τ_{c} is the Coulomb friction, b_{w} is the viscous friction coefficient, and c_{d} is the aerodynamic drag coefficient.

Those parameters were determined experimentally with a torque controller by varying the torque reference, registering

Table 2 Friction torque parameters

Parameter	Value
τ_c	2.46×10^{-3} N·m
b_w	1.06×10^{-5} N·m·s·rad^{-1}
c_d	1.70×10^{-8} N·m·s^2·rad^{-2}

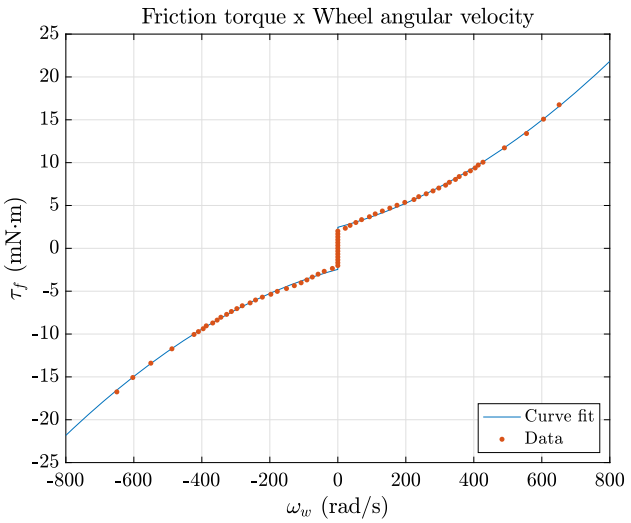

Fig. 7 Friction torque

the equivalent steady-state velocity (where the input torque equals the friction torque) and then making a curve fitting of the data (Fig. 7). The identified parameters are given in Table 2.

4.2 Feedback Linearization

Adopting a new input u and making the input torque τ equal to

$$\tau = -m_c g\, d\, \Gamma q + \tau_f(\omega_w) - \bar{I}_{c_O} u, \tag{30}$$

result in a feedback linearization law that cancels out the gravity torque and motor friction (Fig. 8).

Substituting Eq. (30) in (25) reduces the system to:

$$\begin{cases} \dot{q} = G(q)^T \omega_c \\ \dot{\omega}_c = u \end{cases}. \tag{31}$$

Although the angular velocity differential equation is now linear, the unit complex number differential equation is still nonlinear.

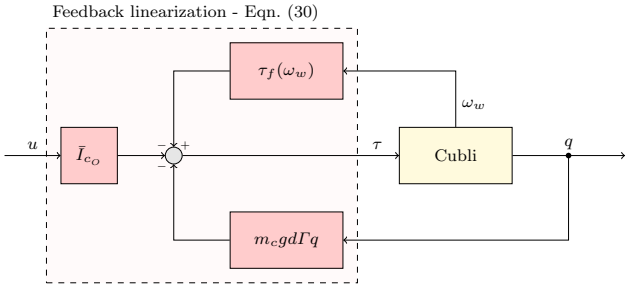

Fig. 8 Cubli with feedback linearization

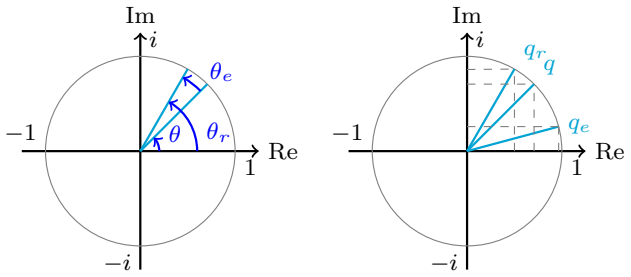

(a) Angle **(b)** Complex number

Fig. 9 Orientation error

4.3 State Regulator

Let q_r be the unit complex number reference and q_e be the unit complex number error, i.e.,

$$q_r = \begin{bmatrix} q_{r_0} \\ q_{r_1} \end{bmatrix}, \qquad q_e = \begin{bmatrix} q_{e_0} \\ q_{e_1} \end{bmatrix}. \tag{32}$$

The orientation error (θ_e) represents the rotation needed for the current orientation (θ) to match the reference orientation (θ_r) (Fig. 9a):

$$\theta_r = \theta + \theta_e. \tag{33}$$

Because unit complex numbers always have unitary norm ($|q_r| = |q| = |q_e| = 1$), in complex number notation, consecutive rotations can be represented as multiplications between respective complex numbers (Fig. 9b), which means that:

$$q_r = q \circ q_e. \tag{34}$$

By left-multiplying both sides of Eq. (34) with $\bar{q}$, it is possible to see that:

$$q_e = \bar{q} \circ q_r. \tag{35}$$

When the current orientation matches the reference orientation, no additional rotation is needed and thus, the unit complex number error is $q_e = [1\ 0]^T$. Because q_e is not

zero (and will never be, since an orientation complex number always has unitary norm), Eq. (36) could not be used to guarantee asymptotically stable error dynamics, i.e.,

$$\ddot{q}_e + k_d \dot{q}_e + k_p q_e \neq \begin{bmatrix} 0 \\ 0 \end{bmatrix}. \tag{36}$$

However, as seen in Eq. (37), the imaginary part of the unit complex number error will be zero, which means that Eq. (37) could be used instead:

$$\ddot{q}_{e_1} + k_d \dot{q}_{e_1} + k_p q_{e_1} = 0. \tag{37}$$

The first time derivative of q_e can be calculated differentiating Eq. (35) and making use of Eq. (24):

$$\begin{aligned} \dot{q}_e &= \frac{d}{dt}\left(\bar{q} \circ q_r\right) \\ &= \dot{\bar{q}} \circ q_r + \bar{q} \circ \cancelto{0}{\dot{q}_r} \\ &= \dot{\bar{q}} \circ (q \circ q_e) \\ &= -\begin{bmatrix} 0 \\ \omega_c \end{bmatrix} \circ q_e \Rightarrow \begin{cases} \dot{q}_{e_0} = \omega_c q_{e_1} \\ \dot{q}_{e_1} = -\omega_c q_{e_0} \end{cases}. \end{aligned} \tag{38}$$

The second time derivative of q_e can be calculated by differentiating Eq. (38):

$$\begin{aligned} \ddot{q}_e &= \frac{d}{dt}\left(-\begin{bmatrix} 0 \\ \omega_c \end{bmatrix} \circ q_e\right) \\ &= -\begin{bmatrix} 0 \\ \dot{\omega}_c \end{bmatrix} \circ q_e - \begin{bmatrix} 0 \\ \omega_c \end{bmatrix} \circ \dot{q}_e \\ &= -\begin{bmatrix} 0 \\ \dot{\omega}_c \end{bmatrix} \circ q_e - \begin{bmatrix} 0 \\ \omega_c \end{bmatrix} \circ \left(-\begin{bmatrix} 0 \\ \omega_c \end{bmatrix} \circ q_e\right) \\ &= -\begin{bmatrix} 0 \\ \dot{\omega}_c \end{bmatrix} \circ q_e - \begin{bmatrix} \omega_c^2 \\ 0 \end{bmatrix} \circ q_e \Rightarrow \begin{cases} \ddot{q}_{e_0} = \dot{\omega}_c q_{e_1} - \omega_c^2 q_{e_0} \\ \ddot{q}_{e_1} = -\dot{\omega}_c q_{e_0} - \omega_c^2 q_{e_1} \end{cases}. \end{aligned} \tag{39}$$

Substituting Eqs. (38) and (39) in (37) results in:

$$\begin{aligned} \ddot{q}_{e_1} + k_d \dot{q}_{e_1} + k_p q_{e_1} &= 0 \\ \left(-\dot{\omega}_c q_{e_0} - \omega_c^2 q_{e_1}\right) + k_d\left(-\omega_c q_{e_0}\right) + k_p q_{e_1} &= 0 \\ \dot{\omega}_c + k_d \omega_c - \left(k_p - \omega_c^2\right)\frac{q_{e_1}}{q_{e_0}} &= 0. \end{aligned} \tag{40}$$

Isolating $\dot{\omega}_c$ yields the following control law:

$$u = \left(k_p - \omega_c^2\right)\frac{q_{e_1}}{q_{e_0}} - k_d \omega_c. \tag{41}$$

The term $\sigma_e = \frac{q_{e_1}}{q_{e_0}}$ is singular for $\pm 90°$ rotations (since the term $q_{e_0} = \cos\theta_e$ appears in the denominator). However, since the objective is to stabilize the Cubli vertically, the biggest possible error would be $\pm 45°$, and probably the actuators would saturate way before that. Moreover, for small rotations, the term ω_c^2 is close to zero and q_{e_0} is close to one, which further simplifies the control law:

$$u \approx k_p q_{e_1} - k_d \omega_c. \tag{42}$$

Also, for small errors, the unit complex number error and angular velocity are approximate to:

$$q_e = \begin{bmatrix} \cos\theta_e \\ \sin\theta_e \end{bmatrix} \approx \begin{bmatrix} 1 \\ \theta_{c_r} - \theta_c \end{bmatrix}, \qquad \omega_c \approx \dot{\theta}_c. \tag{43}$$

Substituting Eq. (43) in (42) yields a state regulator that is equal to the one commonly utilized with angles when dealing with small rotations:

$$u \approx k_p\left(\theta_{c_r} - \theta_c\right) - k_d \dot{\theta}_c. \tag{44}$$

This means that, for small rotations, the derived nonlinear control law of Eq. (41) is equivalent to a linear one dynamically linearized at the reference.

4.4 Controller Gains

Substituting Eq. (41) in (31), and rewriting the first differential equation in terms of σ_e instead of q, yields:

$$\begin{cases} \dot{\sigma}_e = \left(1 + \sigma_e^2\right)\omega_c \\ \omega_c = \left(k_p - \omega_c^2\right)\sigma_e - k_d \omega_c \end{cases}. \tag{45}$$

When the Cubli is in its equilibrium position $\sigma_e = \omega_c = 0$, the closed-loop linearized dynamics are:

$$\begin{bmatrix} \dot{\sigma}_e \\ \dot{\omega}_c \end{bmatrix} = \left[\begin{array}{c:c} 0 & -1 \\ \hdashline k_p & -k_d \end{array}\right]\begin{bmatrix} \sigma_e \\ \omega_c \end{bmatrix}. \tag{46}$$

Its characteristic equation is:

$$s^2 + k_d s + k_p = 0. \tag{47}$$

Comparing Eq. (47) with the characteristic equation of a generic second-order system with two complex poles with damping ratio ζ and natural frequency ω_n:

$$s^2 + 2\zeta\omega_n s + \omega_n = 0, \tag{48}$$

yields the following values for the controller gains in terms of the desired closed-loop parameters ζ and ω_n:

$$\begin{cases} k_p = \omega_n^2 \\ k_d = 2\zeta\omega_n \end{cases}. \tag{49}$$

5 Attitude and Wheel Controller

Since the 1D Cubli configuration is influenced by the acceleration of the reaction wheel, the velocity of the wheel might saturate for a while. Moreover, the structure may not be perfectly symmetric and the attitude sensor may not be perfectly aligned to the structure. So, what might appear to be an equilibrium position may actually not be, and the wheel will be always accelerating trying to keep the 1D Cubli in that position. It is thus desirable to try to achieve the dual goals of stabilizing the 1D Cubli and keep the wheel velocity small.

5.1 State Regulator

To achieve these goals, the control law of Eq. (41) may be slightly modified by also having feedback from the reaction wheel angular displacement and velocity such that

$$u = \left(k_\mathrm{p} - \omega_\mathrm{c}^2\right)\sigma_\mathrm{e} - k_\mathrm{d}\omega_\mathrm{c} - k_{\mathrm{p_w}}\theta_\mathrm{w} - k_{\mathrm{d_w}}\omega_\mathrm{w}. \tag{50}$$

The full nonlinear control law (Fig. 10) is composed of the feedback linearization from Eq. (30) and the state regulator from Eq. (50).

5.2 Controller Gains

Substituting Eq. (50) in (31), and rewriting the first differential equation in terms of σ_e instead of q, yields:

$$\begin{cases} \dot{\sigma}_\mathrm{e} = \left(1+\sigma_\mathrm{e}^2\right)\omega_\mathrm{c} \\ \dot{\theta}_\mathrm{w} = \omega_\mathrm{w} \\ \omega_\mathrm{c} = \left(k_\mathrm{p} - \omega_\mathrm{c}^2\right)\sigma_\mathrm{e} - k_\mathrm{d}\omega_\mathrm{c} - k_{\mathrm{p_w}}\theta_\mathrm{w} - k_{\mathrm{d_w}}\omega_\mathrm{w} \\ \dot{\omega}_\mathrm{w} = \frac{m_\mathrm{c} g d}{I_{\mathrm{w_G}}}\sigma_\mathrm{e} - k_\mathrm{p}\frac{\bar{I}_{\mathrm{c_O}}}{I_{\mathrm{w_G}}}\sigma_\mathrm{e} + k_\mathrm{d}\frac{\bar{I}_{\mathrm{c_O}}}{I_{\mathrm{w_G}}}\omega_\mathrm{c} \\ \qquad\qquad + k_{\mathrm{p_w}}\frac{\bar{I}_{\mathrm{c_O}}}{I_{\mathrm{w_G}}}\theta_\mathrm{w} + k_{\mathrm{d_w}}\frac{\bar{I}_{\mathrm{c_O}}}{I_{\mathrm{w_G}}}\omega_\mathrm{w} \end{cases}. \tag{51}$$

When the 1D Cubli is in its equilibrium position $\sigma_\mathrm{e} = \omega_\mathrm{c} = \theta_\mathrm{w} = \omega_\mathrm{w} = 0$, the closed-loop linearized dynamics can be represented as:

$$\begin{bmatrix} \dot{\sigma}_\mathrm{e} \\ \dot{\theta}_\mathrm{w} \\ \dot{\omega}_\mathrm{c} \\ \dot{\omega}_\mathrm{w} \end{bmatrix} = \left[\begin{array}{c:c:c:c} 0 & 0 & -1 & 0 \\ \hdashline 0 & 0 & 0 & 1 \\ \hdashline k_\mathrm{p} & -k_{\mathrm{p_w}} & -k_\mathrm{d} & -k_{\mathrm{d_w}} \\ \hdashline \frac{m_\mathrm{c} g d}{I_{\mathrm{w_G}}} - k_\mathrm{p}\frac{\bar{I}_{\mathrm{c_O}}}{I_{\mathrm{w_G}}} & k_{\mathrm{p_w}}\frac{\bar{I}_{\mathrm{c_O}}}{I_{\mathrm{w_G}}} & k_\mathrm{d}\frac{\bar{I}_{\mathrm{c_O}}}{I_{\mathrm{w_G}}} & k_{\mathrm{d_w}}\frac{\bar{I}_{\mathrm{c_O}}}{I_{\mathrm{w_G}}} \end{array}\right] \begin{bmatrix} \sigma_\mathrm{e} \\ \theta_\mathrm{w} \\ \omega_\mathrm{c} \\ \omega_\mathrm{w} \end{bmatrix}. \tag{52}$$

Its characteristic equation is:

$$s^4 + \left(k_\mathrm{d} - \gamma k_{\mathrm{d_w}}\right)s^3 + \left(k_\mathrm{p} - \gamma k_{\mathrm{p_w}}\right)s^2 + \delta k_{\mathrm{d_w}} s + \delta k_{\mathrm{p_w}} = 0, \tag{53}$$

where

$$\gamma = \frac{\bar{I}_{\mathrm{c_O}}}{I_{\mathrm{w_G}}}, \qquad \delta = \frac{m_\mathrm{c} g d}{I_{\mathrm{w_G}}}. \tag{54}$$

Comparing Eq. (53) with the characteristic equation of a generic fourth-order system with two complex poles and two repeated real poles:

$$\begin{aligned} &\left(s^2 + 2\zeta\omega_\mathrm{n} s + \omega_\mathrm{n}^2\right)\left(s + \alpha\zeta\omega_\mathrm{n}\right)^2 = 0 \\ &s^4 + 2\zeta\omega_\mathrm{n}\left(1+\alpha\right)s^3 + \omega_\mathrm{n}^2\left(1 + \alpha\zeta^2\left(4+\alpha\right)\right)s^2 \\ &\qquad + \left(2\alpha\zeta\omega_\mathrm{n}^3\left(1+\alpha\zeta^2\right)\right)s + \alpha^2\zeta^2\omega_\mathrm{n}^4 = 0, \end{aligned} \tag{55}$$

yields the following values for the controller gains in terms of the desired closed-loop parameters ζ, ω_n and α:

$$\begin{cases} k_\mathrm{p} = \omega_\mathrm{n}^2\left(1 + \alpha\zeta^2\left(4+\alpha\right)\right) + \gamma\dfrac{\alpha^2\zeta^2\omega_\mathrm{n}^4}{\delta} \\ k_\mathrm{d} = 2\zeta\omega_\mathrm{n}\left(1+\alpha\right) + \gamma\dfrac{2\alpha\zeta\omega_\mathrm{n}^3\left(1+\alpha\zeta^2\right)}{\delta} \\ k_{\mathrm{p_w}} = \dfrac{\alpha^2\zeta^2\omega_\mathrm{n}^4}{\delta} \\ k_{\mathrm{d_w}} = \dfrac{2\alpha\zeta\omega_\mathrm{n}^3\left(1+\alpha\zeta^2\right)}{\delta} \end{cases}. \tag{56}$$

Note that if $\alpha = 0$, the controller gains k_p and k_d are equal to the ones derived in Eq. (49), while the controller gains $k_{\mathrm{p_w}}$ and $k_{\mathrm{d_w}}$ are equal to zero. By choosing a small enough value of α, one guarantees that the reaction wheel dynamics would be slow enough to not interfere in the Cubli dynamics. In other words, the Cubli closed-loop poles will be sufficient faster than the reaction wheel closed-loop poles.

6 Experimental Results

To validate the controller, experiments were realized with the Cubli prototype (Fig. 3). Its electronics is composed of one STM32 NUCLEO-L432KC development board (80MHz ARM 32-bit Cortex M4), one SparkFun 9dof Sensor Stick inertial measurement unit (LSM9DS1), three Maxon EC 45 Flat brushless motors with a Maxon ESCON Module 50/5 dedicated motor controller each and one Turnigy Graphene Panther 1000mAh 6S LiPo battery. It is important to mention that in the 1D configuration, only one pair of motor and reaction wheel is actuated. The microcontroller runs ARM Mbed OS open-source operating system, communicates with the IMU with I2C serial communication protocol and with the motor controllers with PWM and analog signals. A dedicated PCB was built to interface all these components. The

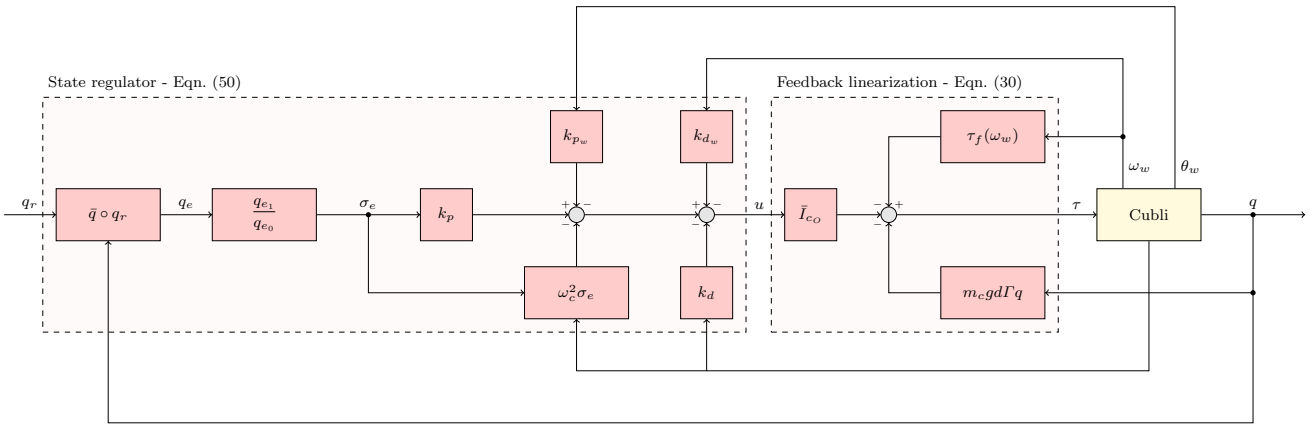

Fig. 10 Cubli with state regulator and feedback linearization

mechanical parts were made in laser cut aluminum and 3D printed ABS.

To estimate the Cubli angular displacement θ_c and angular velocity ω_c, a complementary filter was developed that fuses the accelerometer readings, which has high-frequency noise due to centripetal and tangential accelerations, with the gyroscope readings, which has low-frequency noise due to a constant bias being integrated over time. The wheel angular displacement and angular velocity were obtained from a second-order state observer, which takes into account not only the applied torque τ as well as the motors hall sensors readings.

Experimental results were obtained (Fig. 11), adopting $\zeta = \frac{\sqrt{2}}{2}$, $\omega_n = 1.5\omega_0$ and $\alpha = 0.1$ for the controller gains and setting the unit complex number reference to the unstable equilibrium position $q_r = q_u$, that is, $\theta_{c_r} = 45°$.

The Cubli was released around 15° from the equilibrium position and it was stabilized in less than 1 s, as can be seen for its angular velocity ω_c quickly decaying to zero. The reaction wheel angular velocity ω_w also decayed to zero, but at a much slower rate of around 10 s. This makes sense since $\alpha = 0.1$, which means the Cubli dynamics should be 10 times faster.

Two external disturbances were applied, one around 9 s and the other around 16 s. In both cases, the control system quickly rejected the disturbance without oscillating too much or saturating the actuators, which would happen from torques above 0.5N.m.

Moreover, the 1D Cubli did not stabilize at 45° but around 50°. This probably happened due to construction imperfections or sensor misalignment. However, because the reaction wheel states are also being feedback, the controller was able to find the real equilibrium position.

The experimental data are practically noise-free due to the implementation and tuning of the state estimators previously described.

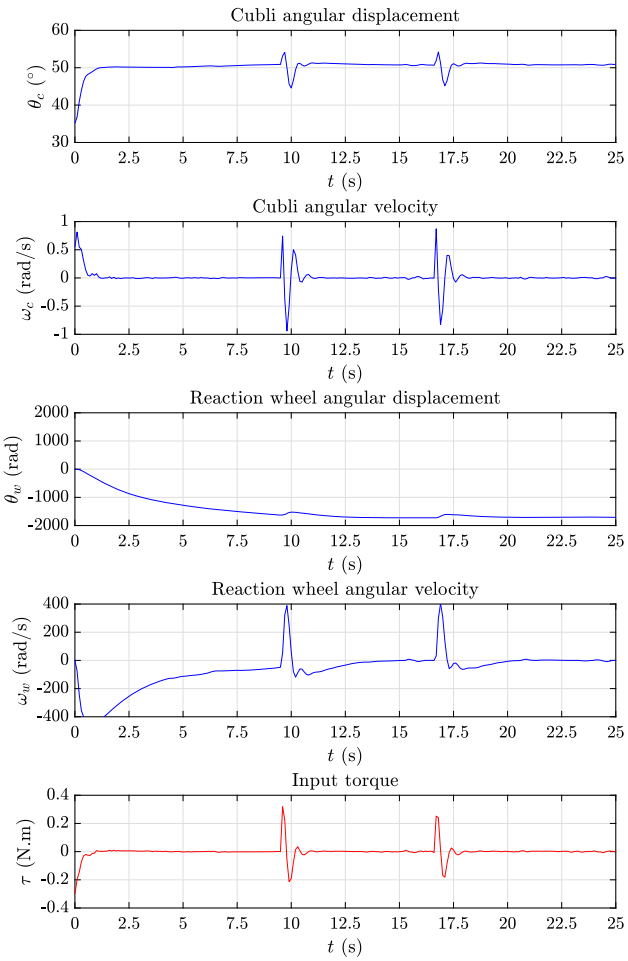

Fig. 11 Experimental results

A video of this and other experiments is available at https://youtu.be/Q2rAg7tytjw.

7 Conclusion

By utilizing unit complex numbers instead of angles, a nonlinear control law was designed and implemented. This approach proved to be efficient given the experimental results of the Cubli balancing on its edge (1D). It has the advantage of not needing any trigonometric operations in the control algorithm, although the computation efficiency gains are not so significant due to recent advances in embedded microprocessors. So, the main contribution of this work was to show that unit complex numbers can be used to model rotational mechanical systems in the plane and to design nonlinear control law in an intuitive way. This approach helps to understand the use of hypercomplex numbers (quaternions) for modeling and control 3D rotational systems, like the Cubli balancing on its vertex.

Acknowledgements The authors would like to thank the financial support received from FAPESP, process n° 2017/22130-4, and CAPES, process n° 88882.333346/2019-01.

Declarations

Conflict of interest The authors declare that they have no conflict of interest.

References

Andrievsky, B. (2011). Global stabilization of the unstable reaction-wheel pendulum. *Automation and Remote Control, 72*(9), 1981–1993.

Bosso, A., Azzollini, I. A., & Baldi, S. (2019). Global frequency synchronization over networks of uncertain second-order kuramoto oscillators via distributed adaptive tracking. In *2019 IEEE 58th conference on decision and control (CDC), IEEE* (pp. 1031–1036).

Chopra, N., & Spong, M. W. (2005). On synchronization of kuramoto oscillators. In *Proceedings of the 44th IEEE conference on decision and control, IEEE* (pp. 3916–3922).

Fantoni, I., Lozano, R., & Spong, M. W. (2001). Stabilization of the reaction wheel pendulum using an energy approach. In *2001 European control conference (ECC), IEEE* (pp. 2552–2557).

Gajamohan, M., Merz, M., Thommen, I., & D'Andrea, R. (2012). The cubli: A cube that can jump up and balance. In *2012 IEEE/RSJ international conference on intelligent robots and systems* (pp. 3722–3727). https://doi.org/10.1109/IROS.2012.6385896

Gajamohan, M., Muehlebach, M., Widmer, T., & D'Andrea, R. (2013). The cubli: A reaction wheel based 3d inverted pendulum. In *2013 European control conference (ECC)* (pp. 268–274). https://doi.org/10.23919/ECC.2013.6669562

Gritli, H., & Belghith, S. (2018). Robust feedback control of the underactuated inertia wheel inverted pendulum under parametric uncertainties and subject to external disturbances: LMI formulation. *Journal of the Franklin Institute, 355*(18), 9150–9191.

Guaracy, F., Pereira, R., & de Paula, C. (2017). Robust stabilization of inverted pendulum using ALQR augmented by second-order sliding mode control. *Journal of Control, Automation and Electrical Systems, 28*(5), 577–584.

Jepsen, F., Soborg, A., Pedersen, A., & Yang, Z. (2009). Development and control of an inverted pendulum driven by a reaction wheel. In *2009 international conference on mechatronics and automation, IEEE* (pp. 2829–2834).

Lee, S. H., Goswami, A. (2007). Reaction mass pendulum (RMP): An explicit model for centroidal angular momentum of humanoid robots. In *Proceedings 2007 IEEE international conference on robotics and automation* (pp. 4667–4672)

Muehlebach, M., & D'Andrea, R. (2017). Nonlinear analysis and control of a reaction-wheel-based 3-d inverted pendulum. *IEEE Transactions on Control Systems Technology, 25*(1), 235–246. https://doi.org/10.1109/TCST.2016.2549266.

Muehlebach, M., Mohanarajah, G., & D'Andrea, R. (2013). Nonlinear analysis and control of a reaction wheel-based 3d inverted pendulum. In *52nd IEEE conference on decision and control* (pp. 1283–1288). https://doi.org/10.1109/CDC.2013.6760059

Roberge, J. K. (1960). *The mechanical seal*. Massachusetts Institute of Technology.

Sanyal, A. K., Chaturvedi, N. A., Bernstein, D., & McClamroch, H. (2004). Dynamics and control of a 3d pendulum. In *43rd IEEE conference on decision and control* (Vol. 1, pp. 323–328).

Shi, P., Wang, H., & Lim, C. C. (2015). Network-based event-triggered control for singular systems with quantizations. *IEEE Transactions on Industrial Electronics, 63*(2), 1230–1238.

Spong, M. W., Corke, P., & Lozano, R. (2001). Nonlinear control of the reaction wheel pendulum. *Automatica, 37*(11), 1845–1851.

Stephenson, A. (1908). *On a new type of dynamical stability*.

Wang, Y., Xia, Y., Shen, H., & Zhou, P. (2017). SMC design for robust stabilization of nonlinear Markovian jump singular systems. *IEEE Transactions on Automatic Control, 63*(1), 219–224.

Xu, X., Lian, C., Zuo, L., & He, H. (2013). Kernel-based approximate dynamic programming for real-time online learning control: An experimental study. *IEEE Transactions on Control Systems Technology, 22*(1), 146–156.

Yang, C., Li, Z., Cui, R., & Xu, B. (2014). Neural network-based motion control of an underactuated wheeled inverted pendulum model. *IEEE Transactions on Neural Networks and Learning Systems, 25*(11), 2004–2016.